Journal of Power Sources Advances 37 (2026) 100200

Contents lists available at ScienceDirect

Journal of Power Sources Advances

journal homepage: www.sciencedirect.com/journal/journal-of-power-sources-advances

Impact of residuals on recovered nickel-rich $LiNi_{1-x-y}Mn_xCo_yO_2$ cathodes for direct recycling and reuse

Mehrdad Talebi [a,b], Thomas Diemant [a,b], Jae-Kwang Kim [c], Markus Binder [a,b,*], Dominic Bresser [a,b,d,**]

[a] Helmholtz Institute Ulm (HIU), 89081, Ulm, Germany
[b] Karlsruhe Institute of Technology (KIT), 76021, Karlsruhe, Germany
[c] Department of Energy Convergence Engineering, Cheongju University, 28503, Cheongju, Republic of Korea
[d] Ulm University (UUlm), 89069, Ulm, Germany

ARTICLE INFO

Keywords:
Recycling
Cathode
Single crystal
Ni-rich NMC
Lithium battery

ABSTRACT

At present, industrial-scale recycling of lithium-ion batteries typically involves rather energy-intensive processes and toxic solvents to recover, in particular, the metallic elements from the positive electrode active material. These recovered metals subsequently serve as precursors for the synthesis of new electrode materials. One approach to reduce the energy and cost needed is the direct recycling of the electrode active materials. Herein, two recovery methods, namely thermal and solvent-based recovery, are investigated for single-crystalline Ni-rich $LiNi_{1-x-y}Mn_xCo_yO_2$ (NMC) high-energy cathodes. The NMC obtained via the thermal recovery method exhibits poor performance due to the generation of HF and the degradation of the material. In contrast, the NMC obtained via the solvent-based method, utilizing dimethyl sulfoxide as a non-toxic solvent, demonstrates superior performance, with a reduction in capacity of only 1.5 % compared to pristine NMC. This comparative analysis highlights the critical role of the separation procedure and, particularly, the detrimental effect of any remaining fluorinated binder.

1. Introduction

The continuous electrification of our modern life, driven by the vast usage of (hybrid) electric vehicles (EVs), portable electronics, and stationary storage systems for renewable energies, has resulted in a severe increase in the demand for lithium-ion batteries (LIBs) [1,2]. Among the various LIB cathode active materials, Ni-rich $LiNi_{1-x-y}Mn_xCo_yO_2$ (Ni-rich NMC) offers very high specific capacity and energy density, with a theoretical capacity in the range of 270 mAh g^{-1}, making it increasingly attractive for high-performance applications [3–6]. Given the high cost of the comprised metals and their scarcity – in particular, nickel and cobalt – waste management of end-of-life LIBs and production waste, such as cathode scrap, has gained increasing attention [7]. Recycling is crucial not only to recover critical elements, but also to reduce the environmental footprint with battery disposal and raw material extraction, as LIB production has increased drastically from 25.6 GWh in 2009 to 218 GWh in 2019, and is estimated to reach 2500 GWh in 2030 [8–10]. Traditional hydrometallurgical and pyrometallurgical methods are suitable to recover elemental constituents, but fail to retain the materials "as they are", i.e., the cathode active material as such with its layered structure and defined particle morphology. In contrast, direct recycling enables the recovery of the cathode active materials with minimal degradation of the structure. More specifically, direct recycling is defined as the recovery and reuse of, e.g., the cathode active material (CAM) from end-of-life (EOL) LIBs without its decomposition into the elemental metals (or any corresponding salt), while retaining the original crystal structure and particle morphology, therefore decreasing energy consumption and lowering the required chemical input in comparison with traditional methods. This leads to a smaller environmental footprint, consuming about ten times less energy and emitting around six times less greenhouse gases compared to hydrometallurgy and pyrometallurgy approaches [11–22]. In addition, scaling direct recycling to an industry level appears quite feasible using, e.g., the froth flotation method, which can separate heavy active material from light conductive

This article is part of a special issue entitled: Battery Recycling published in Journal of Power Sources Advances.

* Corresponding author. Helmholtz Institute Ulm (HIU), 89081, Ulm, Germany.
** Corresponding author. Helmholtz Institute Ulm (HIU), 89081, Ulm, Germany.
E-mail addresses: markus.binder2@kit.edu (M. Binder), dominic.bresser@kit.edu (D. Bresser).

https://doi.org/10.1016/j.powera.2025.100200
Received 4 November 2025; Received in revised form 17 December 2025; Accepted 27 December 2025
Available online 6 January 2026
2666-2485/© 2025 The Authors. Published by Elsevier Ltd. This is an open access article under the CC BY license (http://creativecommons.org/licenses/by/4.0/).

carbon particles [23,24]. However, one of the greatest challenges towards direct recycling is the removal of the binder, polyvinylidene difluoride (PVDF), which is typically used in LIB cathodes [25–28]. PVDF itself is chemically inert, and strongly adheres to the active material and conductive carbon to each other and to the aluminum current collector [29]. During the direct recycling process, though, the incomplete removal of PVDF can lead to impurity accumulation, while at elevated temperatures, its decomposition produces highly active and corrosive byproducts, such as hydrogen fluoride (HF), which can attack the cathode active material, leading to severe structural changes and, thus, negatively affecting the eventual performance of the recovered active material [30–32].

Thermal treatments have been widely explored to simultaneously combust the conductive carbon and decompose the binder, while avoiding HF generation and/or suppressing its reaction with the active material. Several recent studies have suggested heating the electrode in the presence of a second chemical, such as calcium oxide and lithium salts [33,34]. Nonetheless, this potentially results in another contamination source and requires an additional purification step. Additionally, elevated processing temperatures can induce cation mixing in the NMC active material, which means that some Ni^{2+} ions migrate into the lithium layer and occupy Li^{+} ion positions, thereby reducing the electrochemical performance [35]. Moreover, the scalability of the thermal recovery process remains challenging due to the additional energy consumption, environmental concerns, and hazardous gas emissions. Recently, solvent-based recovery methods have gained attention as a more efficient way to remove the binder, especially PVDF, particularly without harming the cathode active material and requiring significantly less energy, while also enabling the recovery of the PVDF binder [17,18]. However, the use of toxic solvents such as *N*-methyl-2-pyrrolidone (NMP) to dissolve and remove PVDF poses environmental concerns [36,37].

Here, dimethyl sulfoxide (DMSO) is introduced as a non-toxic solvent, which can alternatively be used to dissolve and remove the PVDF binder, as it is more biodegradable and less volatile compared to NMP. Despite these positive points, several questions remain, such as the impact of temperature, stirring, and sonication on the PVDF dissolution and removal. Also, the effect of the residual PVDF and conductive carbon in the recovered material has not yet been investigated. Accordingly, a series of thermal recovery and solvent-based recovery protocols using DMSO as the solvent are studied and compared to each other as well as the pristine material. Moreover, the impact of different processing conditions is explored to identify the optimal procedure with regard to the eventual performance of the resulting electrodes. Our findings illustrate that solvent-based recovery using DMSO effectively restores NMC with minimal structural damage and electrode residues, offering a promising and scalable method for recycling PVDF-based NMC cathodes.

2. Experimental section

2.1. Electrode preparation

The NMC cathodes were prepared with the following composition: 92 wt% single-crystalline $LiNi_{0.88}Mn_{0.06}Co_{0.06}O_2$ (SC-NMC88 or simply NMC), 4 wt% of conductive carbon (CNERGY Super C65, Imerys), and 4 wt% polyvinylidene difluoride (PVDF, Solef 6020, Solvay). The PVDF was first dissolved in NMP (anhydrous, 99.5 %, Sigma-Aldrich) to get the binder solution. Then, the mixture of SC-NMC88, conductive carbon, and the binder solution was homogenized using a planetary mixer (ARE-250, Thinky). The slurry was then coated on a battery-grade Al foil using a doctor blade with a wet film thickness of 90 μm for the reference electrodes and 350 μm for recovery purposes. Next, the cathodes were pre-dried at 80 °C for 30 min and subsequently dried overnight in a dry room with a dew point of −70 °C at room temperature. The dried electrodes were cut into disc shapes with a diameter of 12 mm for the reference electrodes and 50 × 50 mm^2 for the recovery process, pressed (Atlas manual hydraulic press, Specac) at 5 tons for 15 s, and finally dried under vacuum (<10^{-3} mbar) at 120 °C for 14 h. The electrodes with the recovered material were prepared with the same procedure and a wet film thickness of 90 μm (analogous to the reference electrodes).

2.2. Thermal recovery process

In this study, pristine coatings are used as electrode scrap, i.e., freshly made cathodes (50 × 50 mm^2) were weighed and placed in a ceramic crucible inside a box furnace (Carbolite CWF 11/23). Four different temperatures were applied: 350, 400, 450, and 500 °C. The heating rate was maintained at 10 K min^{-1}. The samples were held at the target temperature for 5 h under an oxygen flow (~1.8 L min^{-1}). After the thermal treatment, the delaminated black mass was separated from the aluminum foil and collected for the subsequent physicochemical and electrochemical characterization. To investigate potential improvements by an additional washing step, the black mass treated at 450 °C was dispersed in dimethyl sulfoxide (DMSO, 67-68-5, VWR Chemicals) and stirred for 1 h at room temperature. The mixture was then separated by centrifugation (Corning LSE, HERMLE) at 6000 rpm for 5 min. The recovered solid was pre-dried at 80 °C for 30 min, followed by complete drying under vacuum (<10^{-3} mbar) at 120 °C for 12 h.

2.3. Solvent-based recovery process

As for the TR process, freshly made cathodes were immersed in DMSO and further treated using four different procedures. For the first set of samples (SR1), sonication was performed for 15 min. After delamination, the aluminum foil was removed, and an additional 2 h of sonication was applied to dissolve the PVDF binder. However, it was observed that the rather long duration of the first sonication step led to fracturing of the aluminum foil (compare the aluminum foil images for different samples in Fig. S1). Therefore, for the second set of samples (SR2), a modified process was applied in which the cathodes were stirred for 10 min, followed by 5 min of sonication and an additional 10 min of stirring before the aluminum foil was removed. The remaining steps were identical to those used for SR1. Both SR1 and SR2 were processed at room temperature. For the third set of samples (SR3), the cathodes were stirred in DMSO for 2 h, followed by 5 min of sonication and an additional 2 h of stirring, with all steps conducted at 40 °C, prior to the removal of the aluminum foil. The subsequent 2 h of sonication, performed after the removal of the aluminum foil, were also carried out at 40 °C. The fourth set of samples (SR4) was prepared similarly to SR3, but with 2 h of stirring at 90 °C and no sonication step. After the aluminum foil separation, the black mass suspension of SR1 was subjected to four rounds of centrifugation at 1000 rpm for 5 min each. For SR2, SR3, and SR4, four rounds of centrifugation at 1000 rpm for 3 min were applied. For each centrifugation step, fresh DMSO was added to the precipitated solid to aid the separation of the conductive carbon and PVDF. The recovered solids were pre-dried for 30 min at 80 °C and then fully dried under vacuum (<10^{-3} mbar) at 120 °C for 12 h. To check for any potential residual PVDF in the thus recovered NMC, the materials were heated to 500 °C, utilizing the same box furnace used in the thermal recovery process. The resulting material is hereinafter referred to as H-SR.

2.4. Physicochemical characterization

Thermogravimetric analysis (TGA) was conducted using a Netzsch STA 409 PC, increasing the temperature from room temperature up to 800 °C at a heating rate of 10 °C min^{-1} under an oxygen atmosphere. X-ray diffraction (XRD) was carried out with a Bruker D8 Advance (Cu Kα,λ = 0.154 nm). Scanning electron microscopy (SEM) was conducted using a Zeiss Crossbeam XB340 field-emission electron microscope equipped with an energy-dispersive X-ray (EDX) spectroscopy detector

(Oxford Instruments X-Max Xtreme, 100 mm^2, 1–10 kV). For the SEM and EDX analysis, the acceleration voltage was set to 5 and 10 keV, respectively. For X-ray photoelectron spectroscopy (XPS), a Specs XPS system with a Phoibos 150 energy analyzer was used. The spectra were recorded using mono-chromatized Al K_α radiation (300 W, 13 kV) and a pass energy of 30 eV for the detailed measurements. All binding energies were calibrated to the main C1s peak at 284.8 eV. To avoid surface contamination, the samples were transferred in an inert gas atmosphere to the sample load lock of the XPS system. The fitting of the XPS results was done with CasaXPS, using Shirley-type backgrounds and Gaussian-Lorentzian (GL30) peak shapes.

2.5. Electrochemical characterization

Electrochemical characterization was performed using three-electrode Swagelok® cells, with lithium metal foil (500 µm thick, battery-grade, Honjo Metal) as the counter electrode. The cathode active material mass loading was in the range from 5 to 6 mg cm^{-2} for all the cells, and the density and porosity of the electrodes after pressing were around 3.1 g cm^{-3} and 32 %, respectively. Metallic lithium was used as the reference electrode. Cell assembly took place in an argon-filled glove box (MB200B ECO, MBraun) with H_2O and O_2 levels maintained below 0.1 ppm. Glass fiber sheets (Whatman GF/D) served as separator and were saturated with 130 µL of the electrolyte (LP30, 1M $LiPF_6$ in a 1:1 wt mixture of ethylene carbonate (EC) and dimethyl carbonate (DMC), UBE). Galvanostatic cycling was conducted between 3.0 and 4.3 V for the Li||NMC cells. All measurements were carried out at 20 ± 2 °C using a Maccor Battery Tester 4300. A charge/discharge rate of 1C corresponds to a specific current of 220 mA g^{-1}. Generally, for each batch, at least two cells with an identical outcome were tested. For the optimized solvent-based process (SR4), three repetitions have been executed with a total of 6 cells to ensure reproducibility of the best results.

3. Results and discussion

The main objective of this work was the development of an active material recovery procedure for nickel-rich NMC electrode scrap, with minimal residuals of conductive carbon and binder, the highest possible recovery efficiency, as well as the lowest possible active material degradation caused by the recovery treatment. The two most straightforward separation methods are (i) the thermal decomposition of the conductive carbon and the PVDF binder, resulting in NMC powder detached from the Al foil, and (ii) the dissolution of the PVDF binder, enabling the separation of the components by flotation and decantation. The recovery rate was about 95 % in the case of (i) and around 93 % for (ii). An overview of the two processes and the different subsequent treatments is depicted in Fig. 1. The upper blue arrow indicates the solvent-based recovery process (SR) with four different posttreatments, and the lower orange arrow refers to the thermal recovery process (TR) and the different posttreatments. In addition, heat-treated checkup samples were prepared to obtain further insights. Since sonication was damaging the aluminum foil and contaminating the recovery products, it was meaningful to reduce the sonication time and compensate for it by elevating the temperature, as heating was even more effective than sonication to dissolve PVDF inside the DMSO solvent. In fact, in the SR4 sample at 90 °C, which was carried out without sonication, delamination occurred faster. The formula to calculate the recovery rate is presented below.

$$Recovery\ rate\ (\%) = \frac{recovered\ active\ material}{electrode\ mass - Al\ foil - binder\ and\ carbon\ mass} = \frac{m_{recovered\ material}}{m_{electrode} - m_{Al\ foil} - m_{binder\ and\ carbon}}$$

In a first step, TGA was conducted (Fig. S2). According to the results, pristine NMC is stable under the given conditions up to 800 °C, while PVDF decomposes in the range of 300–500 °C, and the conductive carbon burns off at around 650 °C (Fig. S2a). For the sake of energy efficiency, we thus tried to keep the temperature for the thermal recovery

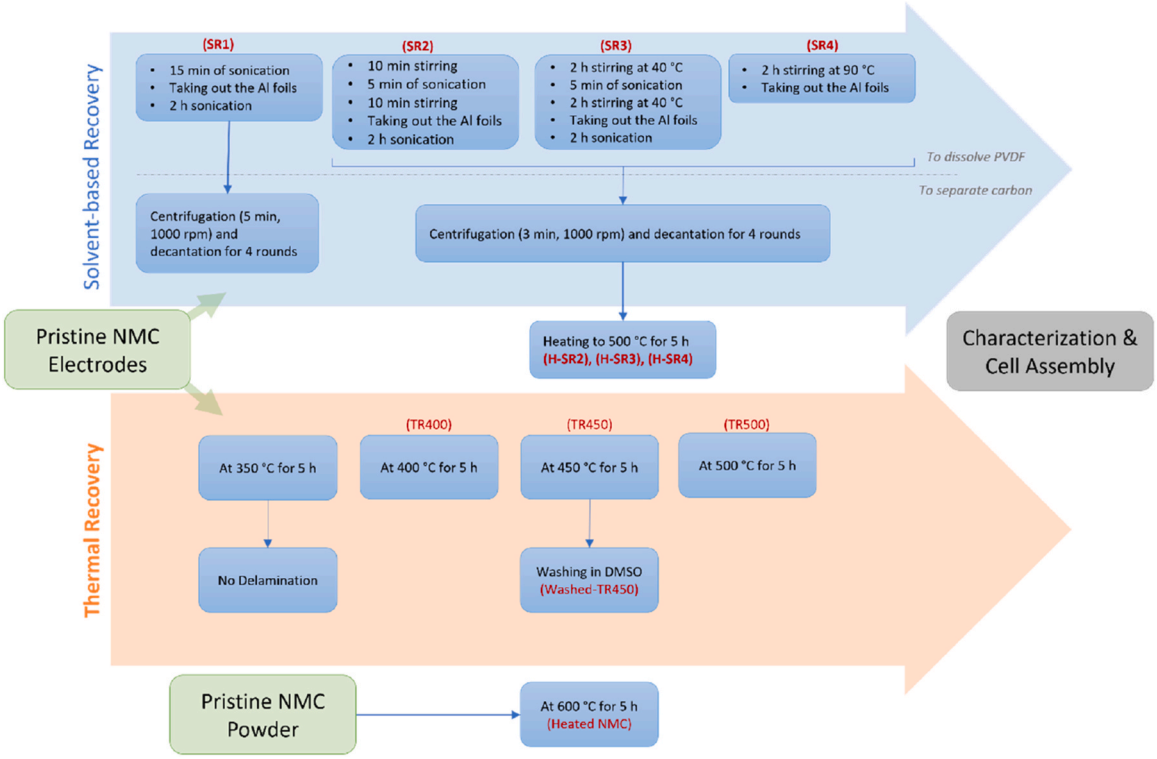

Fig. 1. Overview of the thermal and solvent-based recovery processes.

(TR) as low as possible. In addition, this minimizes the risk of oxygen loss from the NMC lattice [38], even though this is not visible from our TGA results. As a result, we used 350, 400, 450, and 500 °C for the TR process (see Fig. 1). A comparison of the TGA data recorded for the resulting samples is presented in Fig. S2b. The data for TR350 are not shown therein, since there was no delamination of the coating layer observed. For the other three samples, i.e., TR400, TR450, and TR500, there is essentially no mass loss observed; hence, no PVDF or carbon residue can be resolved via TGA. In fact, there is a minor increase in mass for TR450 and TR500 beyond ca. 400 °C, though less than 1 %, indicating that there might be some species present that can be oxidized at elevated temperatures in an oxygen atmosphere. For the SR samples (Fig. S2c), there is essentially no mass loss observed for SR3 and SR4, indicating that these two protocols are capable of removing all binder and conductive carbon. For SR1 and SR2, a little mass loss of about 1.5 % and 2.5 %, respectively, is observed. Interestingly, the mass loss occurs in two steps between 300 and 500 °C. We may assume that this allows for differentiating between residual PVDF and conductive carbon, according to the findings from the differential thermogravimetric analysis (DTG) for the SR samples (Fig. S2) and decomposition graphs of PVDF and conductive carbon in Fig. S2a. Generally, the comparison of these four different SR protocols reveals that a better PVDF dissolution in the first step of the solvent-based recovery also leads to a better carbon separation in the second step (i.e., during the centrifugation). More precisely, the comparison of SR1 and SR2 indicates that the stirring is very effective for the dissolution of PVDF in DMSO, while the comparison with SR3 and SR4 reveals that the application of elevated temperatures further improves the removal of PVDF and the conductive carbon. In fact, only PVDF can be dissolved and separated, yielding a mixture of NMC and conductive carbon that can be directly reused in the manufacturing of new electrodes, thereby simplifying the recovery process. However, in this study, the aim was to develop a method that can also be applied to EOL cathodes in the future. Such EOL cathodes show severe degradation, and hence a calcination step is needed [22]. With the additional carbon separation step, any interference between the calcination and any residuals can be prevented.

Subsequently, the recovered NMC was characterized in detail to identify any potential influence of the recovery procedure on the crystal structure, the particle morphology, and the surface chemistry. While we investigated all materials with most of the characterization techniques used, the focus was on TR450 and SR4, as these showed the best electrochemical cycling performance for each recovery method, as will be discussed later on. A comparison of the XRD patterns and the corresponding Rietveld refinement is presented in Fig. S3. The X-ray diffractogram of the pristine NMC in Fig. S3a shows the expected layered oxide structure (R-3m space group), and the refinement yields lattice parameters, summarized in Table 1, which are in good agreement with the literature [39,40]. Neither for the pristine NMC nor for any of the recovered materials were any additional phases observed, confirming the presence of phase-pure materials. The effect of the thermal treatment as such was studied by subjecting pristine NMC to 600 °C for 5 h (Fig. S3b). The intensity of the reflections, the lattice parameters, and the cation mixing remain essentially the same as for the pristine NMC, indicating that such thermal treatment does not have any significant effect on the crystal structure. Differently, the XRD pattern of TR450 (Fig. S3c) shows some minor deviation. The intensity of the reflections is slightly lower, suggesting a minor disorder induced by the thermal recovery [41]. In line with this observation, the cation mixing is somewhat higher than in the original sample, presumably due to the exposure to the PVDF decomposition products such as HF [42]. Differently, the solvent-recovered sample SR4 (Fig. S3d) closely resembles the diffractogram of the pristine NMC. Overall, the comparison of the intensity, position of the reflections, the lattice parameters, and the cation mixing suggests that the SR process is less harmful for the cathode active material.

Table 1
Comparison of the Rietveld refinement of the XRD data recorded for the pristine, heated, thermally recovered, and solvent-recovered NMC samples.

	c (Å)	a (Å)	c/a	Cation mixing[a] (%)	R_{wp}	GOF
Pristine NMC	14.210 (0)	2.8781 (3)	4.937	2.27 ± 0.07	2.46	2.3
Heated NMC	14.207 (3)	2.8786 (0)	4.935	2.32 ± 0.07	2.38	2.3
TR450	14.214 (4)	2.8798 (2)	4.936	4.53 ± 0.08	2.73	2.6
SR4	14.209 (0)	2.8779 (4)	4.936	1.85 ± 0.07	2.20	2.1

[a] The given error solely refers to the refinement error.

In the next step, we also studied the morphology of the different materials via SEM (Fig. 2). In line with the comparison of the XRD data, the simple thermal treatment of the pristine material (Fig. 2a) did not alter the particle morphology (Fig. 2b). In contrast, the TR process clearly had an impact, resulting in a less smooth particle surface, comparable to an orange peel (Fig. 2c). We may assign this to the presence of PVDF and its temperature-induced, highly corrosive decomposition product HF, which appears to etch the NMC particle surface. In fact, we also observed some smaller solid deposits on the NMC particles, presumably resulting from the reaction of HF and NMC. In order to check the possibility of washing off those surface impurities, we performed a washing step using DMSO. However, the SEM analysis of the washed sample shows that the deposits are still present, and the orange-peel-like texture is also still observed (Fig. 2d). The subsequent EDX analysis (Fig. 2e) reveals a significant fluorine concentration, and the mapping of the fluorine concentration and its overlap with the manganese mapping indicates the formation of manganese fluoride – presumably as a result of the reaction of the NMC active material and HF, as mentioned above. To further confirm the evolution of HF during the thermal recovery process, we also analyzed the delaminated aluminium foil from the thermal recovery process and examined it more closely using SEM and EDX in comparison with a fresh aluminium foil. The results are shown in Fig. S4. The etching of the aluminium foil is clearly visible, and the EDX analysis reveals the presence of fluorine, thus corroborating the previous assumption concerning the decomposition pathway.

Among the solvent-recovered materials, the SEM analysis of SR1 reveals the presence of a significant fraction of conductive carbon and PVDF (Fig. 3a), which is in good agreement with the TGA results (Fig. S2c). Differently, we observe substantially less carbon/PVDF residues for SR2, limited to the boundary between single particles (Fig. 3b), and negligible traces, if any, for SR3 (Fig. 3c) and SR4 (Fig. 3d). It appears that the higher temperature of the DMSO solvent promotes PVDF dissolution and, thus, an improved separation, which also enhances the separation of carbon from NMC during centrifugation.

To further analyze the potential presence of any remaining PVDF and its impact, SR2, SR3, and SR4 were heated to 500 °C for 5 h in order to investigate whether any HF is formed as a decomposition product – comparable to the thermal recovery process. The SEM analysis of these samples did not show any visual degradation, though, as depicted in Fig. S5, and the surface remained flat and smooth – different from the materials resulting from the thermal recovery process (Fig. 2), while the carbon residues (if any) were burnt off.

In a subsequent step, we analyzed the surface chemistry of the recovered materials in more detail by XPS. The XPS data recorded for a pristine electrode containing PVDF as binder (Fig. 4a) show that there is a small amount of LiF detectable already prior to any recovery treatment, likely formed during the slurry preparation and mixing along with the subsequent drying and the presence of surface impurities on the NMC active material [43]. Interestingly, the amount of LiF appears not to increase significantly during the thermal recovery process, while a large amount of metal fluorides is exemplarily detected for TR450 (Fig. 4b) [44–46], which is in very good agreement with the EDX data, suggesting that these metal fluoride species are essentially manganese fluoride. Also remarkably, there is no indication of PVDF in the XPS

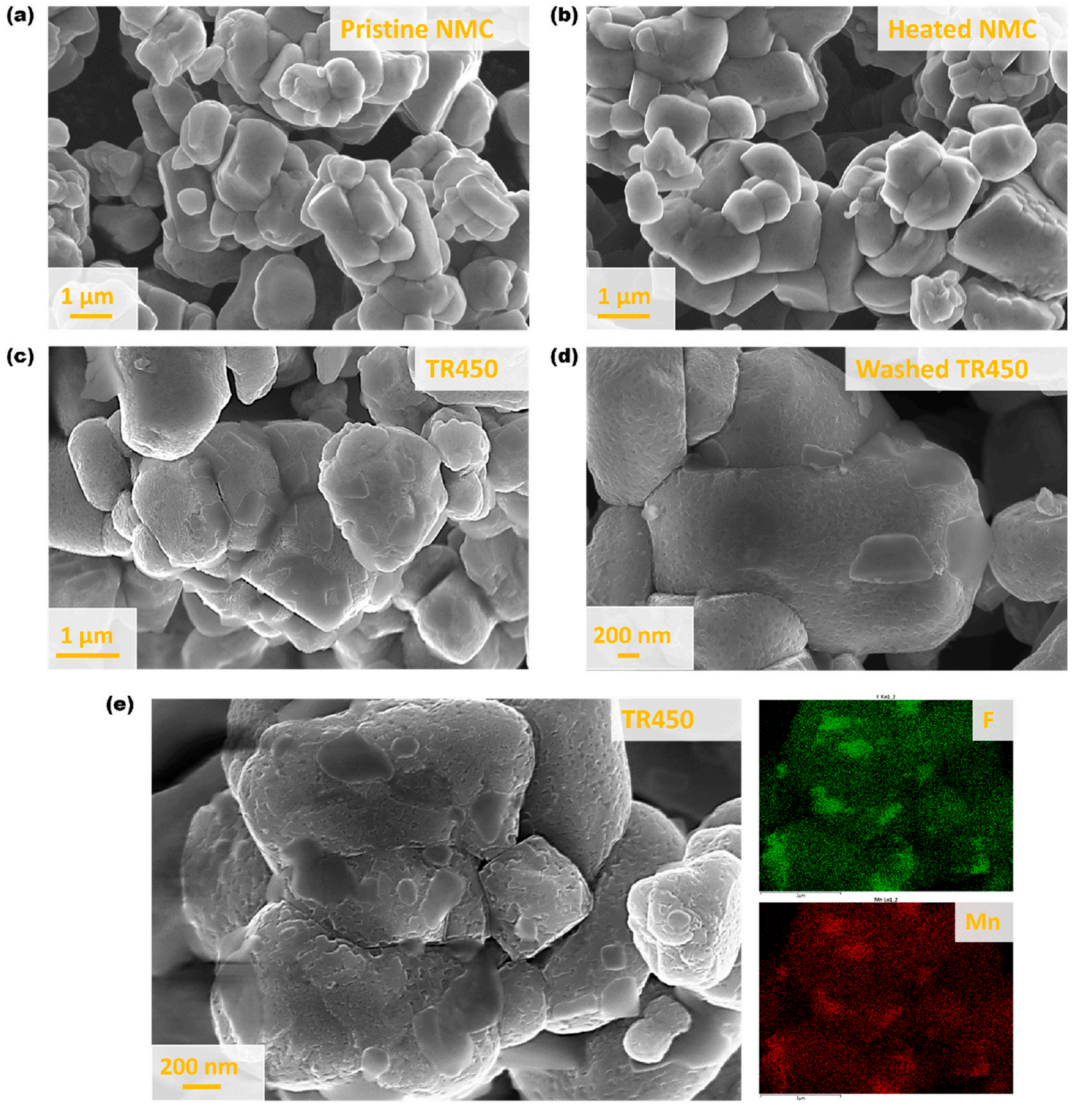

Fig. 2. SEM micrographs of (a) pristine NMC, (b) heated NMC (T = 600 °C), (c) thermally recovered NMC (TR450), and (d) TR450 NMC after washing. (e) SEM micrograph with higher magnification and EDX mapping of fluorine (in green) and manganese (in red) of TR450 after washing.

spectrum anymore, indicating that it has been completely decomposed during the thermal recovery process. For the solvent-recovered material (here exemplarily for SR4; Fig. 4c), it is observed that this approach effectively removes most of the PVDF without forming metal fluoride deposits. The LiF content, however, increases compared to the pristine electrode, possibly due to the processing of NMC and PVDF together in a slurry-like suspension (at an elevated temperature of 90 °C) – just as during the electrode preparation. The higher temperature likely promotes the reaction of NMC and PVDF, leading to the formation of LiF. Such a slight increase in LiF, though, is not necessarily detrimental for the performance as electrode active material – not least, as it is present also in the pristine electrodes, but might be even beneficial potentially for stabilizing the interface with the electrolyte [47]. Nevertheless, the residual PVDF might become an issue during any subsequent thermal treatment. Hence, we evaluated the potential impact of the residual PVDF by subjecting the SR4 material to a thermal treatment at 500 °C (H-SR4). Remarkably, no metal fluoride species were found (Fig. 4d), even though the residual PVDF is burned off, which is in very good agreement with the SEM results. Furthermore, comparing the XPS survey spectra (Fig. 6S) reveals that SR4 and H-SR4 resemble the pristine material, whereas the TR method appeared to be not successful in this regard.

Eventually, we used the recovered materials to prepare new electrodes and subjected these to galvanostatic cycling tests. The results are presented in Fig. 5. The direct comparison of electrodes based on pristine NMC and heated pristine NMC shows that there is essentially no impact of the heat treatment (Fig. 5a). Recovering NMC through the thermal recovery process, however, leads to very poor results and a rapid fading – independent of the processing details. The comparison of the first cycle dis-/charge profiles of TR450 and pristine NMC, presented in Fig. S7a, moreover shows that there is already a substantial capacity loss in the first cycle with an initial Coulombic efficiency of only 72 % compared to 89 % for pristine NMC, accompanied by a high overpotential, which can be attributed to the formation of an insulating surface layer on the NMC particles, caused by the reaction with HF. The washing step leads to some improvement (here depicted for TR450), but the capacity still remains far below the capacity of the pristine NMC electrodes (Fig. 5b). Furthermore, the reproducibility greatly suffers, as illustrated by comparing two different cells with a significant difference in capacity, especially at an elevated C rate of 1C. In contrast, the solvent-based recovery process yields much better performance (Fig. 5c). Among these materials, SR1 shows the poorest performance, most possibly due to the long sonication time and aluminum foil breakage, potentially resulting in additional impurities, as well as the

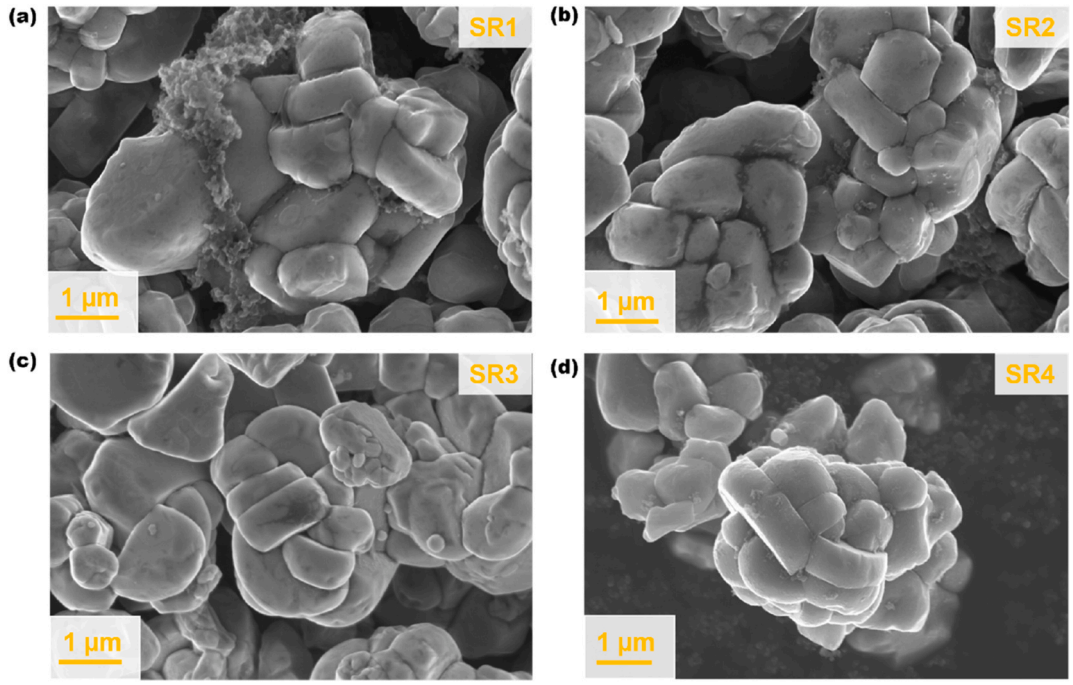

Fig. 3. SEM micrographs of the solvent-recovered samples: (a) SR1, (b) SR2, (c) SR3, and (d) SR4.

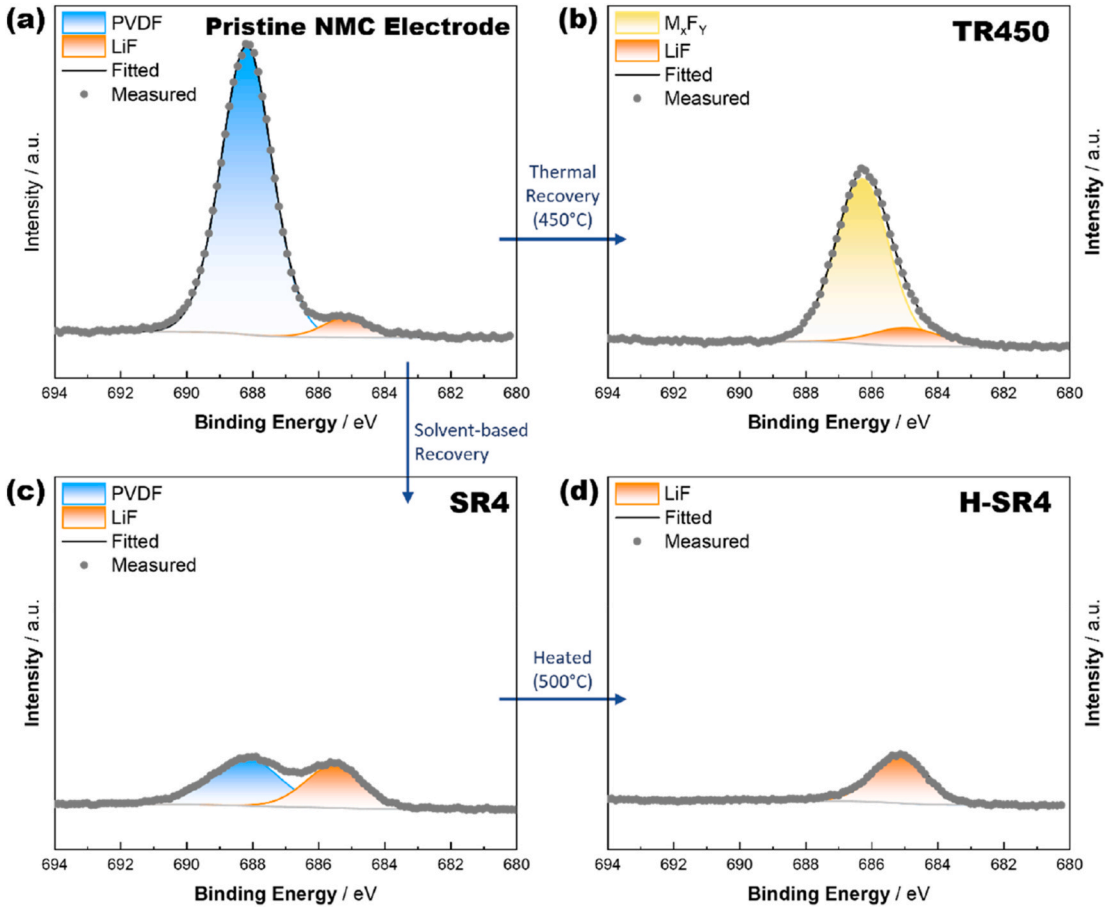

Fig. 4. XPS spectra in the F 1s region of (a) a pristine NMC electrode containing PVDF as binder, (b) a thermally recovered sample (TR450), (c) a solvent-recovered sample (SR4), and (d) a heated solvent-recovered sample (H-SR4).

remaining conductive carbon and PVDF. In fact, SR2 shows already a much better performance in terms of cycling stability and higher specific

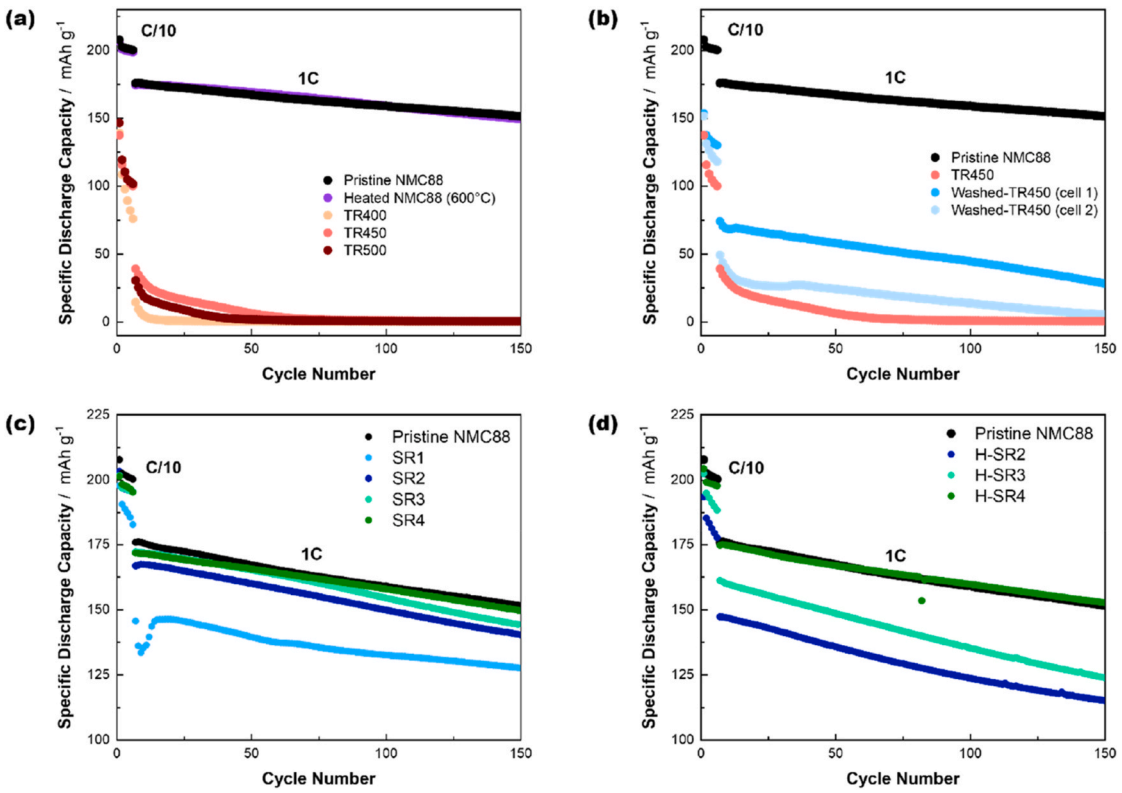

Fig. 5. Galvanostatic cycling of Li||NMC cells at 1C after one formation cycle at C/20 and five cycles at C/10 (cut-off potentials: 3.0 and 4.3 V; all plots also show the results for pristine NMC as reference). (a) Comparison of the thermally recovered (TR) materials and the heated pristine NMC; (b) Comparison of TR450 as the best performing thermally recovered material and washed TR450; (c) Comparison of the solvent-recovered (SR) materials; (d) Comparison of the heat-treated SR materials.

capacities, which is further improved for SR3 and SR4, being in excellent agreement with the SEM and TGA results for this series. SR4 provides essentially the same performance and capacity as the pristine NMC. The comparison of the first cycle dis-/charge profiles of SR4 and pristine NMC, moreover, shows that they are essentially overlapping with a slightly lower reversible capacity in the case of SR4 (Fig. S7b), resulting in an ICE of 84 % – slightly lower than for pristine NMC, but in the same range at least. The analysis of the capacity retention data (Table S1) indicates that the SR samples exhibit values similar to those of the pristine electrode material, with SR4 showing the best performance, reaching a capacity retention of 88 % after 100 cycles at 1C. Comparing the differential capacity (dQ/dV) profiles of the pristine material, TR450, and SR4 (Fig. S8) at C/20 (1st cycle), C/10 (5th cycle), and 1C (20th cycle) reveals the characteristic redox features of the layered oxide structure. The dominant peaks correspond to the H1→H2 and H2→H3 phase transition [48]. The pristine material shows sharp peaks, indicating fast kinetics and high structural order. TR450 exhibits broadened and weaker peaks, reflecting a higher polarization, particularly at higher C rates. In contrast, the solvent-based recovery preserves the redox behavior and the peak positions remain very close to the pristine material. This proves that the elevated temperature (90 °C) is beneficial for dissolving and removing the PVDF binder and, thereby, also the conductive carbon, which is directly reflected in the eventual performance when reused for the preparation of new electrodes. Moreover, the aluminum foils obtained from the SR method might be reused as well, as they are not exposed to HF and, therefore, remain being of high quality and purity. In addition, the carbon and PVDF binder present in the waste DMSO might be recovered through filtration and crystallization, respectively. Consequently, all three components (DMSO, carbon, and PVDF) may be effectively recycled and reused [17,49]. Accordingly, a simple and quick check by TGA can provide a first indication of the quality of a recovery process. In fact, when subjecting the SR materials to an additional heat treatment at 500 °C, the performance of (H-)SR4 is further enhanced, while it has a detrimental impact on (H-)SR3 and (H-)SR2 (Fig. 5d), revealing that even small traces of PVDF (1–2 wt% according to the TGA data) in combination with a treatment at elevated temperatures beyond the common electrode drying temperatures have a severe impact on the performance of the reused electrode material.

4. Conclusion

We systematically investigated two different recovery methods for Ni-rich NMC from electrode scrap, via a thermal and a solvent-based recovery process. The results show that a complete recovery of the conductive carbon and, in particular, the PVDF binder is essential for achieving a suitable performance when reusing the electrode active material in new electrodes. In fact, only a complete removal of PVDF yields a performance comparable to pristine NMC. While the thermal recovery process fails in this regard – not least owing to the temperature-induced reaction of NMC and PVDF, causing the detrimental formation of metal fluorides, especially manganese fluoride, on the particle surface – an optimized solvent-based recovery process, benefitting from the use of DMSO at elevated temperatures, enables the complete removal of PVDF and, thus, a performance that is essentially the same as for the pristine material. Furthermore, it can be concluded that heating the DMSO solvent is more effective than sonication to dissolve PVDF, and sonication can be excluded to prevent further contamination with aluminum foil particles. This study also nicely shows that a simple and quick TGA provides a very good indication of the quality of the recovered material, thus facilitating the recovery at the industrial level. Moreover, we believe that this process can be easily scaled to an industrial level for effectively separating the active material, carbon, and PVDF via froth floatation – potentially also in a continuous fashion.

CRediT authorship contribution statement

Mehrdad Talebi: Writing – review & editing, Writing – original draft, Investigation, Data curation. **Thomas Diemant:** Writing – review & editing, Investigation, Data curation. **Jae-Kwang Kim:** Writing – review & editing, Resources. **Markus Binder:** Writing – review & editing, Writing – original draft, Supervision, Methodology, Data curation, Conceptualization. **Dominic Bresser:** Writing – review & editing, Supervision, Resources, Funding acquisition, Conceptualization.

Declaration of competing interest

The authors declare that they have no known competing financial interests or personal relationships that could have appeared to influence the work reported in this paper.

Acknowledgement

The authors would like to acknowledge financial support from the European Union#180; s Horizon Europe transport program under the SiGNE project (grant agreement No. 101069738) and from the Helmholtz Association.

Appendix A. Supplementary data

Supplementary data to this article can be found online at https://doi.org/10.1016/j.powera.2025.100200.

Data availability

Data will be made available on request.

References

[1] M. Marinaro, D. Bresser, E. Beyer, P. Faguy, K. Hosoi, H. Li, J. Sakovica, K. Amine, M. Wohlfahrt-Mehrens, S. Passerini, Bringing forward the development of battery cells for automotive applications: perspective of R&D activities in China, Japan, the EU and the USA, J. Power Sources 459 (2020) 228073, https://doi.org/10.1016/j.jpowsour.2020.228073.

[2] M. Armand, P. Axmann, D. Bresser, M. Copley, K. Edström, C. Ekberg, D. Guyomard, B. Lestriez, P. Novák, M. Petranikova, W. Porcher, S. Trabesinger, M. Wohlfahrt-Mehrens, H. Zhang, Lithium-ion batteries – current state of the art and anticipated developments, J. Power Sources 479 (2020), https://doi.org/10.1016/j.jpowsour.2020.228708.

[3] Y.S. Chen, R. Dominko, M. Marczewski, W. Wieczorek, Optimizing high-energy lithium-ion batteries: a review of single crystalline and polycrystalline nickel-rich layered cathode materials: performance, synthesis and modification, Appl. Phys. A Mater. Sci. Process. 130 (2024), https://doi.org/10.1007/s00339-024-07897-7.

[4] I.A. Moiseev, A.A. Savina, A.D. Pavlova, T.A. Abakumova, V.S. Gorshkov, E. M. Pazhetnov, A.M. Abakumov, Single crystal Ni-rich NMC cathode materials for lithium-ion batteries with ultra-high volumetric energy density, Energy Adv. (2022) 677–681, https://doi.org/10.1039/d2ya00211f.

[5] F.I. Saaid, M.F. Kasim, T. Winie, K.A. Elong, A. Azahidi, N.D. Basri, M.K. Yaakob, M.S. Mastuli, S.N. Amira Shaffee, M.Z. Zolkiffly, M.R. Mahmood, Ni-rich lithium nickel manganese cobalt oxide cathode materials: a review on the synthesis methods and their electrochemical performances, Heliyon 10 (2024) e23968, https://doi.org/10.1016/j.heliyon.2023.e23968.

[6] J. Fan, H. Luo, T. Wang, S. Dai, Progress in direct recycling of spent lithium nickel manganese cobalt oxide (NMC) cathodes, Energy Storage Mater. 73 (2024) 103813, https://doi.org/10.1016/j.ensm.2024.103813.

[7] E.A. Olivetti, G. Ceder, G.G. Gaustad, X. Fu, Lithium-Ion battery supply chain considerations: analysis of potential bottlenecks in critical metals, Joule 1 (2017) 229–243, https://doi.org/10.1016/j.joule.2017.08.019.

[8] W. Mrozik, M.A. Rajaeifar, O. Heidrich, P. Christensen, Environmental impacts, pollution sources and pathways of spent lithium-ion batteries, Energy Environ. Sci. 14 (2021) 6099–6121, https://doi.org/10.1039/d1ee00691f.

[9] I. Gaalich, I. Driouech, N. Hayagan, C. Aymonier, G. Sonnemann, J. Olchowka, G. Philippot, P. Loubet, Life cycle assessment of an innovative process assisted by pressurized CO2 for direct recycling of lithium-ion battery positive electrode production scraps, ACS Sustain. Chem. Eng. 13 (2025) 4717–4728, https://doi.org/10.1021/acssuschemeng.4c09427.

[10] Y. Lu, J. Wang, Life cycle assessment for spent lithium-ion batteries' recycling process: environmental impact, energy consumption, and sensitivity analysis, ACS Sustain. Chem. Eng. 12 (2024) 12966–12975, https://doi.org/10.1021/acssuschemeng.4c04541.

[11] S. Al-Asheh, A. Aidan, T. Allawi, F. Hammoud, H. Al Ali, M. Al Khamiri, Treatment and recycling of spent lithium-based batteries: a review, J. Mater. Cycles Waste Manag. 26 (2024) 76–95, https://doi.org/10.1007/s10163-023-01842-1.

[12] P. Zheng, D. Young, T. Yang, Y. Xiao, Z. Li, Powering battery sustainability: a review of the recent progress and evolving challenges in recycling lithium-ion batteries, Front. Sustain. Resour. Manag. 2 (2023), https://doi.org/10.3389/fsrma.2023.1127001.

[13] Y. Yao, M. Zhu, Z. Zhao, B. Tong, Y. Fan, Z. Hua, Hydrometallurgical processes for recycling spent lithium-ion batteries: a critical review, ACS Sustain. Chem. Eng. 6 (2018) 13611–13627, https://doi.org/10.1021/acssuschemeng.8b03545.

[14] M.M. Gnutzmann, A. Makvandi, B. Ying, J. Buchmann, M.J. Lüther, B. Helm, P. Nagel, M. Peterlechner, G. Wilde, A. Gomez-Martin, K. Kleiner, M. Winter, J. Kasnatscheew, Direct recycling at the material level: unravelling challenges and opportunities through a case study on spent Ni-Rich layered oxide-based cathodes, Adv. Energy Mater. (2024) 2400840, https://doi.org/10.1002/aenm.202400840.

[15] A. Pražanová, Z. Plachý, J. Kočí, M. Fridrich, V. Knap, Direct recycling technology for spent lithium-ion batteries: limitations of current implementation, Batteries 10 (2024), https://doi.org/10.3390/batteries10030081.

[16] V. Gupta, X. Yu, H. Gao, C. Brooks, W. Li, Z. Chen, Scalable direct recycling of cathode black mass from spent lithium-ion batteries, Adv. Energy Mater. 13 (2023) 1–8, https://doi.org/10.1002/aenm.202203093.

[17] A. Sarkar, R. May, S. Ramesh, W. Chang, L.E. Marbella, Recovery and reuse of composite cathode binder in lithium ion batteries, ChemistryOpen 10 (2021) 545–552, https://doi.org/10.1002/open.202100060.

[18] M. Ahuis, A. Aluzoun, M. Keppeler, S. Melzig, A. Kwade, Direct recycling of lithium-ion battery production scrap – solvent-based recovery and reuse of anode and cathode coating materials, J. Power Sources 593 (2024) 233995, https://doi.org/10.1016/j.jpowsour.2023.233995.

[19] Y. Cao, J. Li, H. Ji, X. Wei, G. Zhou, H.M. Cheng, A review of direct recycling methods for spent lithium-ion batteries, Energy Storage Mater. 70 (2024) 103475, https://doi.org/10.1016/j.ensm.2024.103475.

[20] M.L. Machala, X. Chen, S.P. Bunke, G. Forbes, A. Yegizbay, J.A. de Chalendar, I. L. Azevedo, S. Benson, W.A. Tarpeh, Life cycle comparison of industrial-scale lithium-ion battery recycling and mining supply chains, Nat. Commun. 16 (2025), https://doi.org/10.1038/s41467-025-56063-x.

[21] L. Gaines, J. Zhang, X. He, J. Bouchard, H.E. Melin, Tracking flows of end-of-life battery materials and manufacturing scrap, Batteries 9 (2023), https://doi.org/10.3390/batteries9070360.

[22] L. Gaines, Q. Dai, J.T. Vaughey, S. Gillard, Direct recycling R&D at the recell center, Recycling 6 (2021) 1–18, https://doi.org/10.3390/recycling6020031.

[23] T.O. Folayan, A.L. Lipson, J.L. Durham, H. Pinegar, D. Liu, L. Pan, Direct recycling of blended cathode materials by froth flotation, Energy Technol. 9 (2021) 1–8, https://doi.org/10.1002/ente.202100468.

[24] M. Olutogun, A. Vanderbruggen, C. Frey, M. Rudolph, D. Bresser, S. Passerini, Recycled graphite for more sustainable lithium-ion batteries, Carbon Energy 6 (2024) 1–10, https://doi.org/10.1002/cey2.483.

[25] D.L. Thompson, J.M. Hartley, S.M. Lambert, M. Shiref, G.D.J. Harper, E. Kendrick, P. Anderson, K.S. Ryder, L. Gaines, A.P. Abbott, The importance of design in lithium ion battery recycling-a critical review, Green Chem. 22 (2020) 7585–7603, https://doi.org/10.1039/d0gc02745f.

[26] M. Bhar, S. Ghosh, S. Krishnamurthy, Y. Kaliprasad, S.K. Martha, A review on spent lithium-ion battery recycling: from collection to black mass recovery, RSC Sustain. 1 (2023) 1150–1167, https://doi.org/10.1039/d3su00086a.

[27] E.C. Giles, A. Jarvis, A.T. Sargent, P.A. Anderson, P.K. Allan, P.R. Slater, Direct recycling of EV production scrap NMC532 cathode materials, RSC Sustain. 2 (2024) 3014–3021, https://doi.org/10.1039/d4su00389f.

[28] B.J. Ross, M. Leresche, D. Liu, J.L. Durham, E.U. Dahl, A.L. Lipson, Mitigating the impact of thermal binder removal for direct Li-Ion battery recycling, ACS Sustain. Chem. Eng. 8 (2020) 12511–12515, https://doi.org/10.1021/acssuschemeng.0c03424.

[29] M. Wang, K. Liu, J. Yu, Q. Zhang, Y. Zhang, M. Valix, D.C.W. Tsang, Challenges in recycling spent lithium-ion batteries: spotlight on polyvinylidene fluoride removal, Glob. Chall. 7 (2023), https://doi.org/10.1002/gch2.202200237.

[30] F. Tanaka, L. Gungaajav, O. Terakado, S. Kuzuhara, R. Kasuya, Dehydrofluorination behavior of poly(vinylidene fluoride) during thermal treatment using calcium carbonate, Thermochim. Acta 702 (2021) 178977, https://doi.org/10.1016/j.tca.2021.178977.

[31] M. Huang, M. Wang, L. Yang, Z. Wang, H. Yu, K. Chen, F. Han, L. Chen, C. Xu, L. Wang, Correction: direct regeneration of spent lithium-ion battery cathodes: from theoretical study to production practice, Nano-Micro Lett. 16 (2024) 225, https://doi.org/10.1007/s40820-024-01434-0.

[32] M.C. Rehwoldt, Y. Wang, F. Xu, P. Ghildiyal, M.R. Zachariah, High-temperature interactions of metal oxides and a PVDF binder, ACS Appl. Mater. Interfaces 14 (2022) 8938–8946, https://doi.org/10.1021/acsami.1c20938.

[33] M. Wang, Q. Tan, L. Liu, J. Li, A facile, environmentally friendly, and low-T, ACS Sustain. Chem. Eng. 7 (2019) 12799–12806, https://doi.org/10.1021/acssuschemeng.9b01546.

[34] Y. Ji, C.T. Jafvert, N.N. Zyaykina, F. Zhao, Decomposition of PVDF to delaminate cathode materials from end-of-life lithium-ion battery cathodes, J. Clean. Prod. 367 (2022), https://doi.org/10.1016/j.jclepro.2022.133112.

[35] H. Ronduda, M. Zybert, A. Szczęsna-Chrzan, T. Trzeciak, A. Ostrowski, D. Szymański, W. Wieczorek, W. Raróg-Pilecka, M. Marcinek, On the sensitivity of the ni-rich layered cathode materials for li-ion batteries to the different calcination conditions, Nanomaterials 10 (2020) 1–21, https://doi.org/10.3390/nano10102018.

[36] D. Marchese, C. Giosuè, A. Staffolani, M. Conti, S. Orcioni, F. Soavi, M. Cavalletti, P. Stipa, An overview of the sustainable recycling processes used for lithium-ion batteries, Batteries 10 (2024), https://doi.org/10.3390/batteries10010027.
[37] R. Sliz, J. Valikangas, H. Silva Santos, P. Vilmi, L. Rieppo, T. Hu, U. Lassi, T. Fabritius, Suitable cathode NMP replacement for efficient sustainable printed Li-Ion batteries, ACS Appl. Energy Mater. 5 (2022) 4047–4058, https://doi.org/10.1021/acsaem.1c02923.
[38] M. Ahangari, B. Szalai, J. Lujan, M. Zhou, H. Luo, Advancements and challenges in high-capacity Ni-Rich cathode materials for lithium-ion batteries, Materials 17 (2024), https://doi.org/10.3390/ma17040801.
[39] H. Rostami, P. Mehdipour, T. Hu, P. Molaiyan, P. Tynjälä, U. Lassi, Enhancing the performance of Ni-rich Li[Ni0.88Co0.09Mn0.03]O2 cathode material using surface coating, Sustain. Energy Fuels 9 (2025) 3041–3054, https://doi.org/10.1039/d5se00052a.
[40] L. Zheng, J.C. Bennett, M.N. Obrovac, All-dry synthesis of single crystal NMC cathode materials for Li-Ion batteries, J. Electrochem. Soc. 167 (2020) 130536, https://doi.org/10.1149/1945-7111/abbcb1.
[41] A. Rensmo, E.K. Savvidou, I.T. Cousins, X. Hu, S. Schellenberger, J.P. Benskin, Lithium-ion battery recycling: a source of per- and polyfluoroalkyl substances (PFAS) to the environment? Environ. Sci. Process. Impacts 25 (2023) 1015–1030, https://doi.org/10.1039/d2em00511e.
[42] Y. Wang, Y. Zheng, Different effects of impurities on recovered cathode materials from hydrometallurgical recycling. ECS Meet. Abstr, 2022, p. 590, https://doi.org/10.1149/MA2022-015590mtgabs. MA2022-01.
[43] A. Laurita, L. Zhu, P.E. Cabelguen, J. Auvergniot, D. Guyomard, P. Moreau, N. Dupré, Residual Li2O degrades PVdF during the preparation of NMC811 slurries for Li-ion batteries, Chem. Commun. 59 (2023) 4951–4953, https://doi.org/10.1039/d3cc00471f.
[44] R. Ma, Y. Zhou, L. Yao, G. Liu, Z. Zhou, J.M. Lee, J. Wang, Q. Liu, Capacitive behaviour of MnF2 and CoF2 submicro/nanoparticles synthesized via a mild ionic liquid-assisted route, J. Power Sources 303 (2016) 49–56, https://doi.org/10.1016/j.jpowsour.2015.10.102.
[45] F. Liu, Y. Liu, D. Gao, S. Ma, S. Zhang, Y. Li, J. Zhang, Y. Xue, C. Tang, Designing a MnF2/MnO2 heterostructure for enhanced electrocatalysis in the oxygen reduction reaction, Colloids Surf. A Physicochem. Eng. Asp. 688 (2024) 1–8, https://doi.org/10.1016/j.colsurfa.2024.133637.
[46] M. Hekmatfar, I. Hasa, R. Eghbal, D.V. Carvalho, A. Moretti, S. Passerini, Effect of electrolyte additives on the LiNi0.5Mn0.3Co0.2O2 surface film formation with lithium and graphite negative electrodes, Adv. Mater. Interfac. 7 (2020) 1–13, https://doi.org/10.1002/admi.201901500.
[47] B.P. Thapaliya, T. Wang, A.Y. Borisevich, H.M. Meyer, X.G. Sun, M. P. Paranthaman, C.A. Bridges, S. Dai, In situ ion-exchange metathesis induced conformal LiF surface films on cathode (NMC811) as a cathode electrolyte interphase, Adv. Funct. Mater. 33 (2023) 1–11, https://doi.org/10.1002/adfm.202302443.
[48] G. Nuroldayeva, D. Adair, Z. Bakenov, B. Uzakbaiuly, Revealing phase transition in Ni-Rich cathodes via a nondestructive entropymetry method, ACS Omega 8 (2023) 37899–37907, https://doi.org/10.1021/acsomega.3c03245.
[49] Y. Fu, X. Dong, B. Ebin, Resource recovery of spent lithium-ion battery cathode materials by a supercritical carbon dioxide system, Molecules 29 (2024), https://doi.org/10.3390/molecules29071638.